atmosphere

Article

Assessment of Typhoon Precipitation Forecasts Based on Topographic Factors

Xu-Zhe Chen [1], Yu-Long Ma [2,*], Chun-Qiao Lin [1] and Ling-Li Fan [1,3,*]

[1] College of Ocean and Meteorology, Guangdong Ocean University, Zhanjiang 524088, China; 2112102003@stu.gdou.edu.cn (X.-Z.C.); 2112202032@stu.gdou.edu.cn (C.-Q.L.)
[2] Guangdong-Hong Kong-Macao Greater Bay Area Weather Research Center for Monitoring Warning and Forecasting, Shenzhen 518040, China
[3] South China Sea Institute of Marine Meteorology, Guangdong Ocean University, Zhanjiang 524088, China
* Correspondence: mayulong@gbamwf.com (Y.-L.M.); fanll@gdou.edu.cn (L.-L.F.); Tel.: +86-755-883-98247 (Y.-L.M.); +86-759-239-6055 (L.-L.F.)

Abstract: For this paper, a new global atmospheric model (Global-to-Regional Integrated forecast SysTem; GRIST) with improved sub-grid scale orographic parameterization was verified and assessed, with an emphasis on the precipitation caused by typhoons. Four typical typhoon cases were selected for the verification of the model. The results indicate that, compared to the control experiments, the sensitivity experiments consistently simulated the trends in the three-hour cumulative precipitation changes and the high-value regions of total precipitation better. However, the improved experiments only had an ameliorating effect on the cumulative precipitation modelling biases for Typhoon LEKIMA and Typhoon HAGUPIT, not all of them. Precipitation bias is smaller on flat land than that on mountainous land, but the precipitation bias on windward/leeward slopes depends on the typhoon case. Precipitation modelling accuracy varies considerably between flat and mountainous terrain but very little between windward and leeward slopes. The precipitation simulation is poor for all terrains, with large precipitation thresholds in three typhoon cases, but for Typhoon HOTA, after improving the terrain, the model has the ability to forecast the heavy rainfall scenarios of the mountainous terrain.

Keywords: typhoon precipitation; forecast skill; model evaluation; topography

Citation: Chen, X.-Z.; Ma, Y.-L.; Lin, C.-Q.; Fan, L.-L. Assessment of Typhoon Precipitation Forecasts Based on Topographic Factors. *Atmosphere* **2023**, *14*, 1607. https://doi.org/10.3390/atmos14111607

Academic Editors: Nina Nikolova and Martin Gera

Received: 26 September 2023
Revised: 19 October 2023
Accepted: 24 October 2023
Published: 26 October 2023

1. Introduction

Tropical cyclones cause serious economic losses and pose a threat to people's lives and health [1–3]. After a tropical cyclone creates landfall, the topography of the coastal region affects typhoon precipitation through mechanisms such as the excitation of sub-mesoscale eddies and forced uplift [4]. Significant spatial differences in precipitation occur under the influence of topography, and there is a close link between typhoon precipitation and topographic distribution after landfall [5].

Scholars use typhoon numerical forecasting techniques to conduct in-depth research on the influence of topography on typhoon precipitation [6–8]. Woojin Cho et al. [9] found that water vapour is forced upward by topography in typhoons, enhancing precipitation on windward slopes and hilltops. Liu et al. [10] suggested that topography can induce secondary circulation, which can lead to increased precipitation. Yu et al. [11] indicate that mountains promote convection and increase precipitation intensity. Ouyang et al. [12] proposed that as rainbands pass through mountain topography, warm and moist air is lifted up onto steep slopes, causing unstable energy to accumulate on windward slopes, which contributes to precipitation generation in these areas. However, these conclusions were based on single typhoon case studies, and the question of whether they are specific or not remains.

The traditional test of precipitation is an important method for quantitatively assessing the model's ability to forecast precipitation. Based on the dichotomous contingency table [13], skill scores such as the probability of detection(POD), the equitable threat score (ETS) [14], false alarm ratio (FAR), and the critical success index(CSI) [15] have been developed. However, due to the "double-penalty" issues [16,17], such traditional point-to-point scoring cannot better assess spatial forecasts of precipitation in high-resolution models, so tools such as neighbourhood methods [18,19], scale separation methods [20], and field deformation methods [21,22] have been developed to assess precipitation forecasts in high-resolution models [23]. In particular, the neighbourhood method evaluates the probability of precipitation at grid points within a neighbourhood by choosing a certain neighbourhood radius, and it is able to derive the deviation of the spatial forecast of precipitation within the neighbourhood radius [24]. In addition, precipitation model scores calculated on the basis of a neighbourhood dichotomous contingency table can also characterise the precipitation forecasts from the high-resolution model [25,26]. The model precipitation forecast test and evaluation not only help improve the model but also aid in understanding the forecasting capability of extreme precipitation and promote improvements in forecasting levels [27–29]. Typhoon precipitation simulations based on different models have been evaluated and analysed mostly based on individual typhoon cases to explore the mechanisms by which topography influences typhoon precipitation [30,31]. In other words, when a typhoon passes over complex terrain, it can result in heavy local precipitation due to dynamic factors. Previous authors have also quantitatively assessed and analysed the topographic influences on precipitation based on different regions [32–34]. Then, is there any uncertainty regarding the influence of topography on precipitation following typhoons? Typhoons are specific. Terrain data can be optimised to improve precipitation simulations based on numerical model experiments. There have been few quantitative assessments regarding the effects of different terrains on typhoon precipitation, and there is a need for an in-depth assessment of the models for forecasting typhoon precipitation in different terrains.

2. Data and Methods

This paper examines and evaluates the forecast performance of the model on a 3 h cumulative precipitation basis for individual typhoon cases. In order to investigate whether there are commonalities in precipitation across the topography of different typhoons, we screened four individual typhoon cases, namely Typhoon HOTA, HAGUPIT, LEKIMA, and INFA, which are severe socio-economic hazards and pass through complex terrain after landfall but with inconsistent areas of activity. In addition, controlled and sensitivity experiments were set up to verify the general applicability of optimising terrain data to improve precipitation simulation.

2.1. Data

In order to compare the model's ability to forecast precipitation over different terrains, the time period and spatial area (within a 400 km radius of the typhoon centre) where precipitation is heavier of each typhoon were selected for this study (Table 1). The International Best Track Archive for Climate Management (IBTrACS v04) provided the TC Best Track dataset from the Joint Typhoon Warning Center (JTWC) (Pearl Harbor, HI, USA); GPM IMERG Final Precipitation data with a spatial resolution of $0.1^{\circ} \times 0.1^{\circ}$, topographic data with a resolution of $10''$, and station wind field information were provided by the Shanghai Typhoon Institute (Shanghai, China).

2.2. Method

We developed a new global atmospheric model (Global-to-Regional Integrated forecast SysTem; GRIST: A22.5.1) [35] with improved sub-grid scale orographic parameterization, which we set out to verify and assess. The control and sensitivity experiment used the same physical scheme. The physics schemes included the Tiedtke–Bechtold scheme, diagnostic cloud fraction parameterization, the Rapid Radiative Transfer Model for General Circulation

Models Applications (RRTMG), the parameterization scheme for the Yonsei University (YSU), surface layer (Sfclay) parameterizations, and the Noah with multiparameterization (Noah-MP) land surface model. For the sensitivity tests, the grid terrain was based on WRFv4.4 gravity wave drag (GWD) parameterization scheme improvement.

Table 1. Summary of typhoon events.

Event	Period Averaged	3 h Comparisons
HOTA (2017)	0000 UTC 23 Aug. to 0000 UTC 24 Aug.	3 h update frequency: 8 valid times total
LEKIMA (2019)	1200 UTC 9 Aug. to 0000 UTC 11 Aug.	3 h update frequency: 12 valid times total
HAGUPIT (2020)	0000 UTC 3 Aug. to 0000 UTC 4 Aug.	3 h update frequency: 8 valid times total
INFA (2021)	1500 UTC 24 Jul. to 0300 UTC 26 Jul.	3 h update frequency: 12 valid times total

Based on the 10″ resolution elevation data or the terrain height output from the model, the terrain slope of each grid was calculated. This slope was then combined with the wind direction to determine the windward and leeward slope of each grid point at a given moment. Mountainous and flat areas were divided using a threshold of 500 m above sea level. Experiments were conducted to improve the simulation of individual typhoon cases by reducing the terrain smoothness to make it more closely resemble real conditions.

The traditional point-to-point assessment method and the neighbourhood spatial assessment test method were used to assess the model's forecasting capability for different terrains and different magnitudes of precipitation. The neighbourhood radius were used to calculate the equitable threat score (ETS), the probability of detection (POD), the fractions skill score (FSS), and other test parameters based on the dichotomous contingency table, and the 3 h accumulated precipitation was classified into four magnitudes: light rain or above (greater than 0.1 mm), moderate rain or above (greater than 3 mm), heavy rain or above (greater than 10 mm), and torrential rain or above (greater than 20 mm). The differences in the forecast results before and after model simulation improvements were compared. The traditional assessment methods evaluated overall precipitation forecasting capability, while neighbourhood spatial assessment methods highlighted the spatial differences in precipitation. Neighbourhood scoring represents a shift from traditional grid-based scoring to 'region-to-region' scoring within an outwardly expanding neighbourhood centred on a grid point [25]. The fractions skill score (FSS) is one of the tests within the neighbourhood method [36,37] which transforms the forecast field and the real field into the probability distribution field of the grid points to calculate the spatial forecasting capability of each grid point at different precipitation thresholds and within different neighbourhood radii. The FSS was defined as follows:

$$\mathrm{FSS} = 1 - \frac{\frac{1}{\mathrm{N}}\sum_{\mathrm{N}}(\mathrm{P_{fcst}} - \mathrm{P_{obs}})^2}{\frac{1}{\mathrm{N}}\left(\sum_{\mathrm{N}}\mathrm{P_{fcst}^2} - \sum_{\mathrm{N}}\mathrm{P_{obs}^2}\right)}, \quad (1)$$

where $\mathrm{P_{fcst}}$ and $\mathrm{P_{obs}}$ denote the probability of precipitation in the forecast field and the probability of precipitation in the observed field within the radius of the neighbourhood, respectively. N is the number of neighbourhood window areas in the scoring region. A larger FSS indicates a better match between the forecast and the frequency of events in the radius of the neighbourhood of the real situation. The minimum scale with forecasting skill for different precipitation thresholds (and different terrains) was discriminated using the $\mathrm{FSS_u}$ defined by Roberts et al. [38]. The $\mathrm{FSS_u}$ was defined as follows:

$$\mathrm{FSS_u} = \frac{1 + \mathrm{F_{obs}}}{2}, \quad (2)$$

where $\mathrm{F_{obs}}$ represents the percentage rate of actual precipitation over the entire test area.

3. Statistical Characteristics of Precipitation and Forecasting Tests for Different Terrains

3.1. Distribution of Cumulative Typhoon Precipitation

The study of typhoon precipitation characteristics under different topographies begins with identifying the region influenced by each individual typhoon. This involves screening for periods of heavy precipitation before and after each typhoon's landfall. It was observed that there is a complex terrain area covered by typhoon precipitation during each study period. Figure 1 shows China's topography in the region of typhoon landfall.

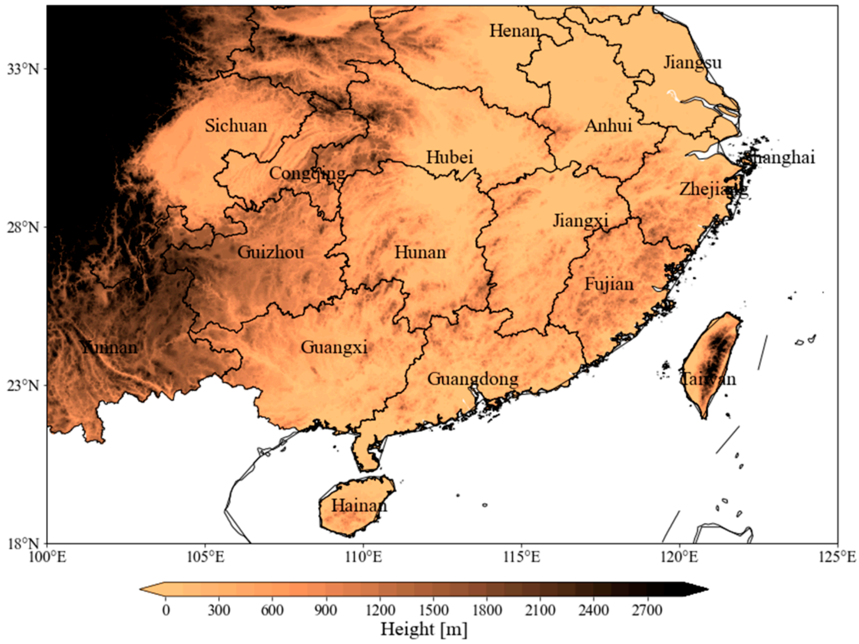

Figure 1. China's topography in the region of typhoon landfall.

Figure 2 shows the distribution of the observed cumulative precipitation, the cumulative precipitation in control experiments, and the cumulative precipitation in sensitivity experiments for four typhoon cases. For Typhoon HOTA, the observed cumulative precipitation covers most of Guangdong, Hainan, and Guangxi, while the range of simulated precipitation is smaller. The gradient of simulated cumulative precipitation is larger than observed, with significant differences between simulated and observed precipitation in the central and western regions of Guangxi. In addition, although the coverage of cumulative precipitation after the model improvement still differs somewhat from the observed data, the extent of the area of large values of cumulative precipitation is much closer to the actual situation than the control experiments. For Typhoon LEKIMA, the model's improved precipitation simulations are closer to the observed precipitation than in the control experiments, with precipitation mainly being concentrated in Zhejiang and Taiwan Island. For Typhoon HAGUPIT, observed precipitation occurred mainly in Northern Taiwan and southern Zhejiang, but the model simulations over-predicted precipitation in western Zhejiang. The model-simulated cumulative precipitation distribution of Typhoon INFA is in good agreement with the observed precipitation, but the observed cumulative precipitation is around 90 mm in the large value area, while the model-simulated precipitation can reach a maximum of over 210 mm, which means that the maximum value of the model-simulated cumulative precipitation is higher than that observed. When considering the cumulative precipitation distribution for the four individual cases, the model generally agrees with the areas of large-value cumulative precipitation compared to the observations. However, the model-simulated precipitation is higher than that observed, and the sensitivity experiments tended to produce more precipitation than the control experiments.

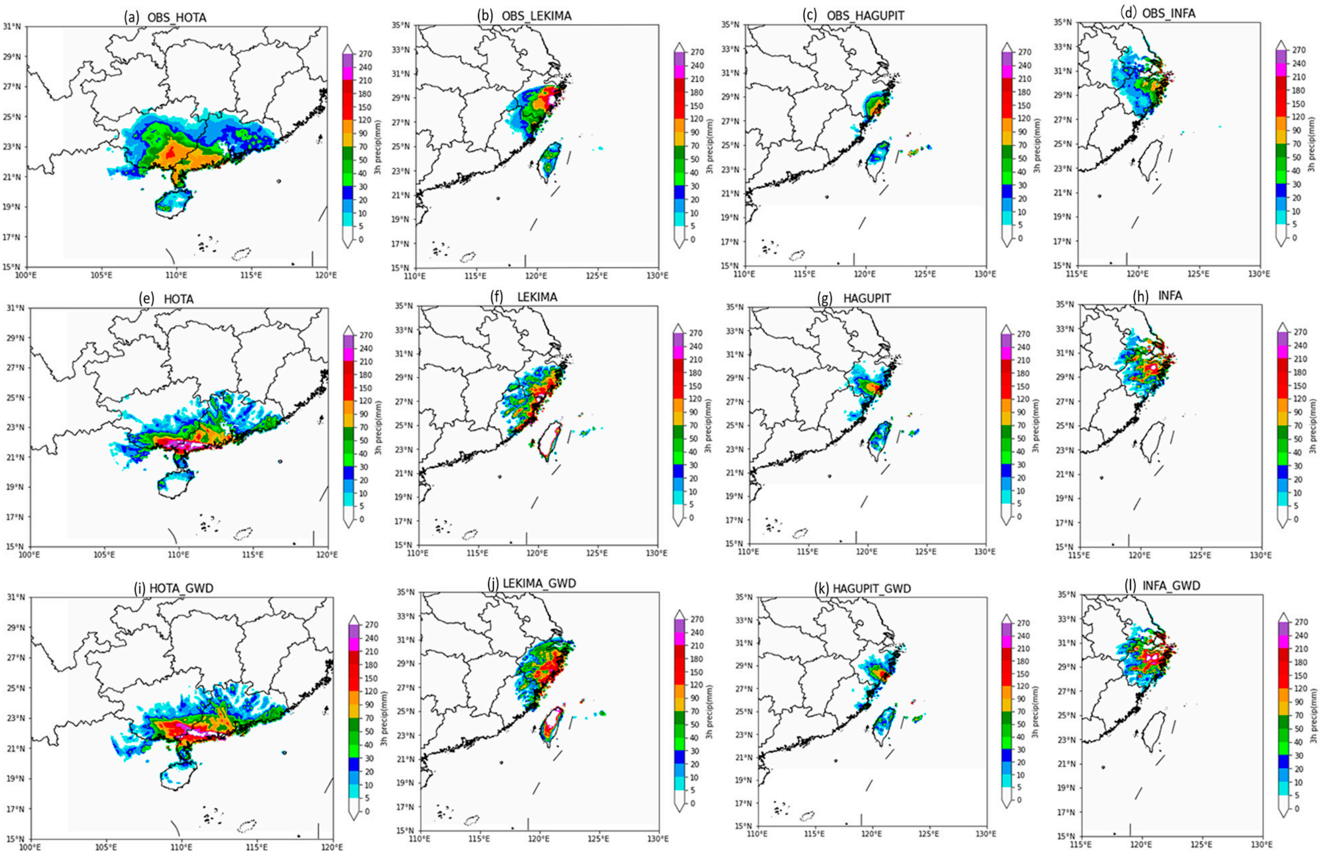

Figure 2. Distribution of observed cumulative precipitation (**a**–**d**), cumulative precipitation of the control experiments (**e**–**h**), and cumulative precipitation of the sensitivity experiments (**i**–**l**) for Typhoon HOTA, Typhoon LEKIMA, Typhoon HAGUPIT, and Typhoon INFA.

3.2. Categorizing Precipitation Patterns and Biases

To quantitatively analyse the mean and deviation of model precipitation, GPM precipitation data were interpolated into the grid of the GRIST model outputs as observed precipitation (Figure 3). Although the Typhoon HOTA flatland precipitation mean was much higher than the mountain precipitation mean, the mountain precipitation deviation was higher than the flatland before and after model improvement. The model-simulated precipitation values for Typhoon HAGUPIT, Typhoon LEKIMA, and Typhoon INFA were significantly greater than the observed precipitation in all terrains both in the control experiments and sensitivity experiments. Typhoon HAGUPIT and Typhoon LEKIMA showed greater precipitation bias on the windward slopes than on the leeward slopes both before and after model improvement, while the opposite was true for Typhoon INFA. Shifts in the precipitation bias relationship between Typhoon HOTA on the windward and leeward slopes before and after the model improvement were observed. Among the four typhoons, the model has the smallest deviation in simulated precipitation for Typhoon HAGUPIT, with only a 1.1 mm deviation in mountainous terrain being recorded before terrain improvement. After terrain improvement, this deviation was further reduced to 0.5 mm. However, the model exhibited the largest deviation in simulated precipitation for Typhoon LEKIMA, exceeding 12 mm in mountainous terrain before terrain improvement. For the poorly modelled Typhoon LEKIMA, the model's simulated precipitation bias was somewhat reduced after decreasing the level of terrain smoothing. On the other hand, for the other typhoon individual cases, improving the terrain is likely to increase the model's precipitation bias. When considering different terrain conditions, all precipitation simulation biases are larger in mountainous areas than in flat areas, but there are individual differences in the precipitation bias of the typhoons on windward and leeward slopes.

Figure 3. Mean (**a**,**c**,**e**,**g**,**i**,**k**,**m**,**o**) and deviation (**b**,**d**,**f**,**h**,**j**,**l**,**n**,**p**) of three-hourly cumulative precipitation for typhoons over different terrains in the control experiments (**a**–**d**,**i**–**l**) and the sensitivity experiments (**e**–**h**,**m**–**p**). (**a**,**b**,**e**,**f**) Typhoon HOTA; (**c**,**d**,**g**,**h**) Typhoon LEKIMA; (**i**,**j**,**m**,**n**) Typhoon HAGUPIT; (**k**,**l**,**o**,**p**) Typhoon INFA.

3.3. Evaluating Cumulative Precipitation Based on Traditional Method

We composed four scenarios with windward/leeward slopes and mountainous/flat terrain. We used the traditional point-to-point assessment method to calculate the equitable threat score (ETS) [14] for light, moderate, heavy, and torrential rainfall magnitudes for each typhoon's 3 h forecast during the test period (Figure 4). ETS values are generally larger (indicating better performance) at lower precipitation thresholds because the model tends to predict low-intensity and high-frequency events accurately. Among the four typhoon examples, all of them except Typhoon HAGUPIT exhibit much higher ETSs for the windward and leeward slopes in flat areas than for mountainous areas. This suggests that the effect of topographic differences between flat and mountainous areas on the model-simulated precipitation is much greater than that of the topographic differences between the windward and leeward slopes and that the model simulates precipitation more accurately for flat areas than for mountainous areas. The scores of the windward and leeward slopes vary considerably from one typhoon case to another, indicating that the impact magnitude varies somewhat from one typhoon case to another. The ETSs for precipitation simulated by the sensitivity experiments are higher. With improved topography, the precipitation scores improved relative to the precipitation scores before the improved topography, especially for the mountainous terrain, with high precipitation thresholds for Typhoon HOTA, and the improved topography significantly improved its precipitation simulation capability.

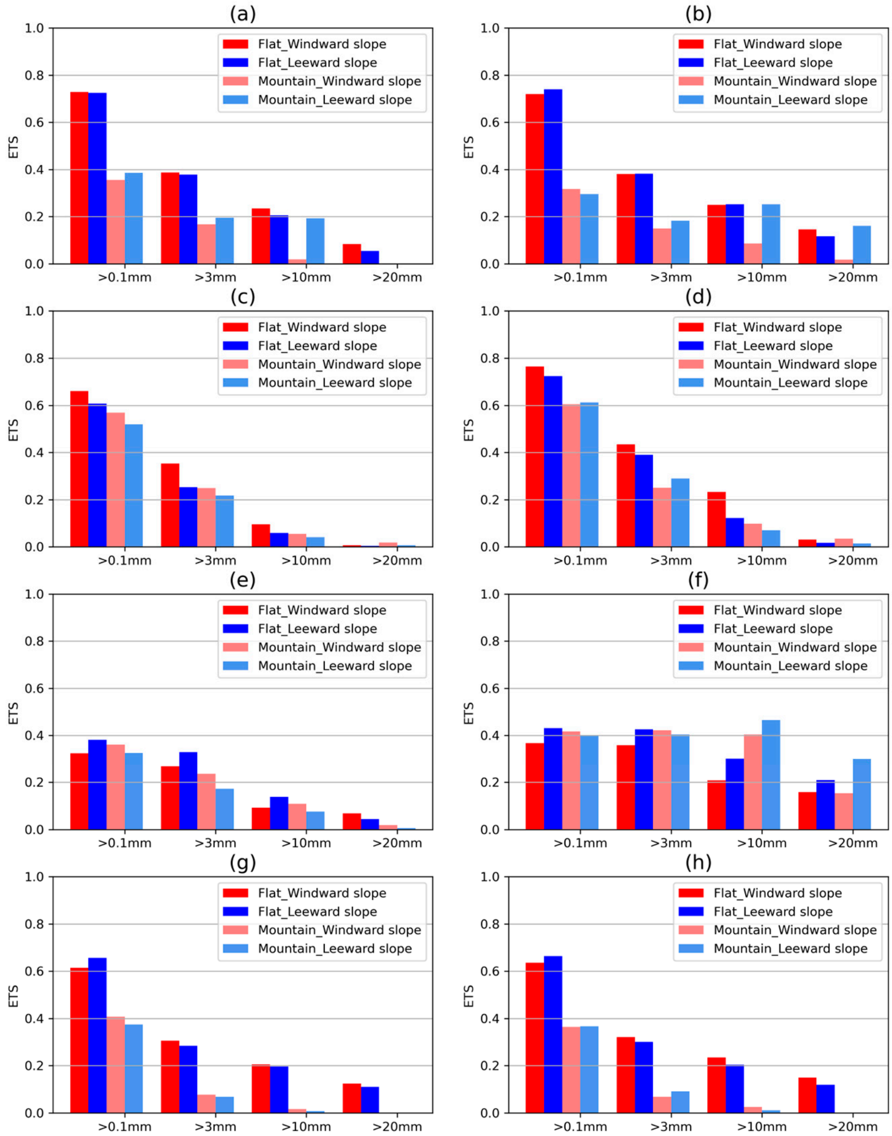

Figure 4. The equitable threat scores (ETSs) of the simulated (**a**,**c**,**e**,**g**) and modified (**b**,**d**,**f**,**h**) experiments for forecasting light, moderate, heavy, and torrential rainfall for three-hourly cumulative precipitation in the test period. (**a**,**b**) Typhoon HOTA; (**c**,**d**) Typhoon LEKIMA; (**e**,**f**) Typhoon HAGUPIT; (**g**,**h**) Typhoon INFA.

To explore the differences in the modelled precipitation simulations before and after the improved topography from multiple perspectives, we also calculated the probability of detection (POD) (Figure 5) and false alarm ratio (FAR) (Figure omitted). The model's ability to forecast typhoon precipitation in the experiment with improved terrain was greatly improved compared to the control experiment, especially for heavy and torrential rainfall. However, the results somewhat depended on how well the typhoon tracks were modelled, which once again demonstrates variations among different individual typhoons. In general, improved terrain experiments are beneficial for enhancing typhoon precipitation modelling. In the control experiments, Typhoon HOTA had 0 hits for storms on mountains, resulting in very poor forecasting levels for mountain storm scenarios. This improved with the introduction of better terrain modelling (Figure 5a,b). Typhoon HAGUPIT's ability to forecast precipitation in the experiment with improved terrain was significantly enhanced compared to the control experiment (Figure 5c,d), especially for heavy and torrential rainfall. In the heavy rainfall scenario, the ETS increased from 0.1 to over 0.3; the POD increased from 0.2 to 0.4 on flat land and rose to over 0.6 on mountainous land, with a significant reduction in FAR. On the other hand, Typhoon INFA did not significantly improve the precipitation forecasting capability due to the improved terrain, especially in the mountainous storm scenario, and the hits did not change before and after the improved experiment (Figure 5e,f). Typhoon HOTA has greater ETS and POD on the leeward slopes of the mountains compared to the windward slopes of the mountains, along with smaller FAR on the leeward slopes of the mountains. The opposite trend was observed for the other typhoon cases (Figure 5g,h). This result depends somewhat on how well the typhoon tracks are modelled and once again highlights the variations among the different individual typhoons. However, in general, improved terrain experiments are beneficial for enhanced typhoon precipitation modelling.

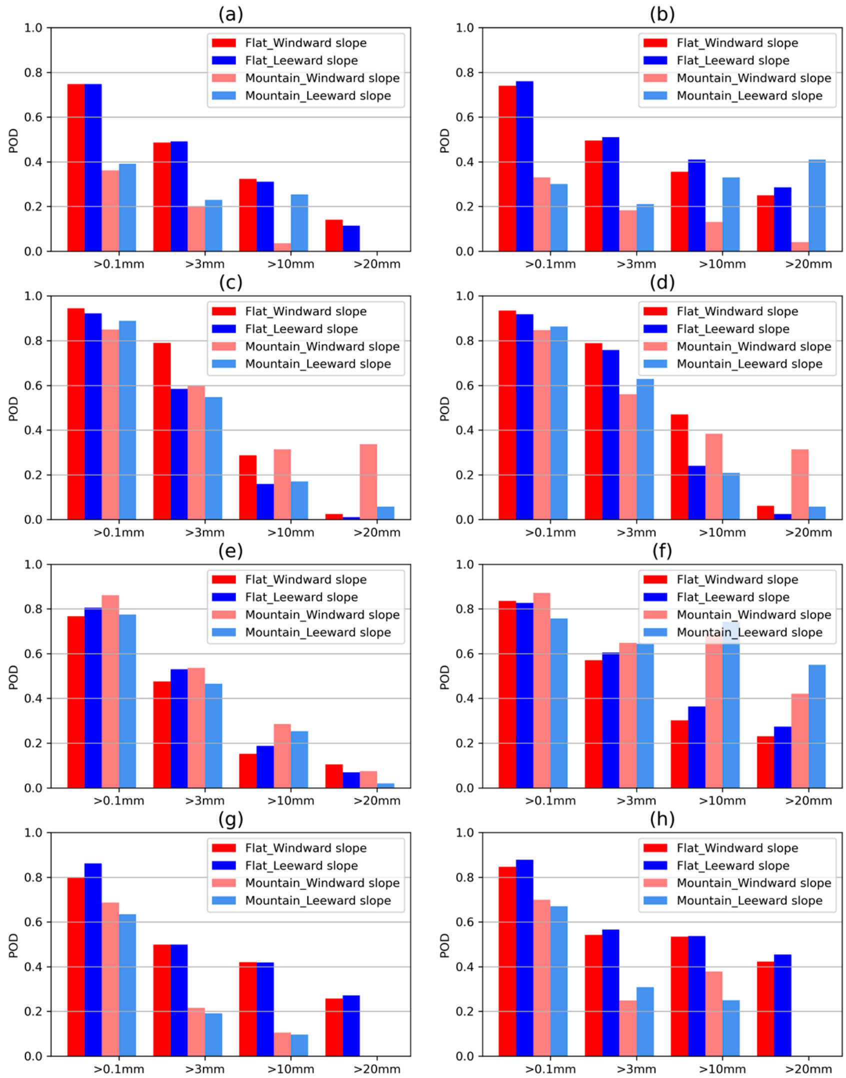

Figure 5. The probability of detection (POD) values of the simulated (**a**,**c**,**e**,**g**) and modified (**b**,**d**,**f**,**h**) experiments for forecasting light, moderate, heavy, and torrential rainfall for three-hourly cumulative precipitation in the test period. (**a**,**b**) HOTA; (**c**,**d**) LEKIMA; (**e**,**f**) HAGUPIT; (**g**,**h**) INFA.

3.4. Evaluating Neighbourhood Cumulative Precipitation

The model-simulated precipitation can differ somewhat from the spatial distribution of observed precipitation due to shifts in the location of the rainbands. Therefore, relying solely on conventional scoring in a high-resolution model has limitations. Researchers have developed methods to evaluate precipitation forecasts in high-resolution models [23], including the neighbourhood method [17–19,24], the scale separation method [20], and field deformation methods [21,22], for simulating the spatial evaluation of precipitation. To quantitatively analyse the spatial characteristics of the four typhoon cases, our paper adopted the neighbourhood method with varying neighbourhood radii to calculate Fractional Skill Score (FSS) under different precipitation thresholds and across different topographies (Figures 6 and 7). Higher FSSs at lower precipitation thresholds, even with small neighbourhood radii, may be due to the greater frequency of lower precipitation thresholds. However, this also indicates that there is not much spatial variation in precipitation at small-precipitation thresholds. In contrast, increasing the neighbourhood radius via using a larger precipitation threshold results in a less significant change in the FSS, which may even still be smaller than the FSS under uniform conditions (FSS_u). In general, under different precipitation thresholds and different terrain conditions, the sensitivity experiments improve the spatial bias of typhoon precipitation. The spatial distribution of precipitation on the mountainous terrain has large error. This implies that the spatial distribution of precipitation on mountainous terrain is highly biased, and the simulation of the precipitation distribution on flat terrain after improving the topography is the most accurate. The FSSs for the windward and leeward slopes still show varying performances among the different typhoons, suggesting that the spatial differences in their precipitation simulations depend on the characteristics of the specific typhoon. This finding is consistent with the results described in Section 3.1.

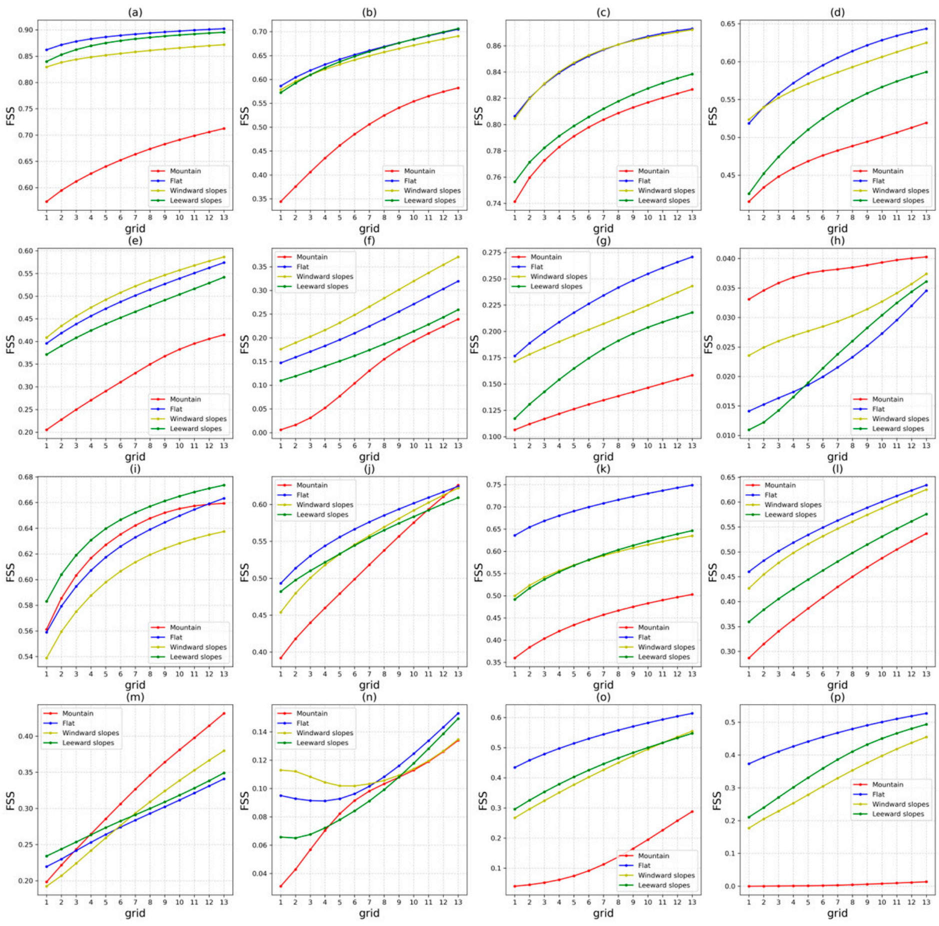

Figure 6. Variation curves of FSS in the control experiments with window area scale under light rain (**a**,**c**,**i**,**k**), moderate rain (**b**,**d**,**j**,**l**), heavy rain (**e**,**g**,**m**,**o**), and torrential rain (**f**,**h**,**n**,**p**) conditions. (**a**,**b**,**e**,**f**) HOTA; (**c**,**d**,**g**,**h**) LEKIMA; (**i**,**j**,**m**,**n**) HAGUPIT; (**k**,**l**,**o**,**p**) INFA.

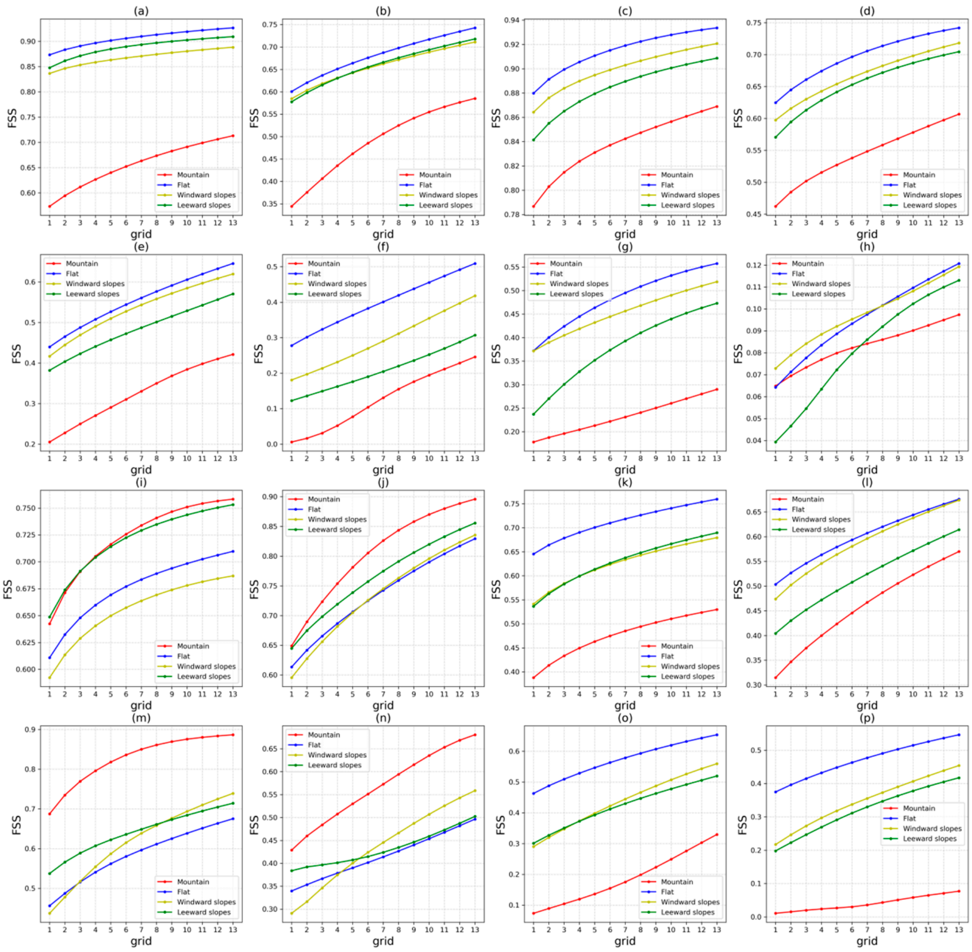

Figure 7. Variation curves of FSS in the sensitivity experiments with window area scale under light rain (**a**,**c**,**i**,**k**), moderate rain (**b**,**d**,**j**,**l**), heavy rain (**e**,**g**,**m**,**o**), and torrential rain (**f**,**h**,**n**,**p**) conditions. (**a**,**b**,**e**,**f**) HOTA; (**c**,**d**,**g**,**h**) LEKIMA; (**i**,**j**,**m**,**n**) HAGUPIT; (**k**,**l**,**o**,**p**) INFA.

Increasing the neighbourhood radius improves the FSS [25,26]. When the precipitation threshold is not large, the FSS for a neighbourhood radius of 13 grid points essentially passes the test for FSS_u [39]. With this in mind, we calculated the critical success index (CSI) (Figure 8) and the bias score (BIAS) (Figure omitted) for the neighbourhood space test using a neighbourhood radius of 13 grid points. There were no significant differences in two-by-two combinations of windward/leeward slopes and mountain/flat terrain types. Therefore, they were simply categorised into four terrain scenarios: windward slopes, leeward slopes, mountainous terrain, and flat terrain. For Typhoon LEKIMA, the CSI converged to 1, and BIAS values were close to 1 for all precipitation thresholds. It is evident that precipitation within this radius was modelled very accurately (Figure 8c,d). In the scenarios of light and moderate rain, CSI was consistently close to 0.8. The simulation was also good, with the exception of Typhoon INFA, which slightly underperformed. However, precipitation simulation was slightly lacking for all terrains with large precipitation thresholds, with Typhoon INFA's performance being particularly poor for heavy and torrential rainfall. INFA's precipitation modelling consistently resulted in more misses and nulls than hits, and the number of misses was greater than the number of nulls (Figure 8g,h). Similarly, precipitation simulations in the neighbourhood were more accurate for flat land than for mountainous terrain. In the sensitivity experiments, precipitation simulation within the neighbourhood tended to improve, but typhoon INFA's performance worsened.

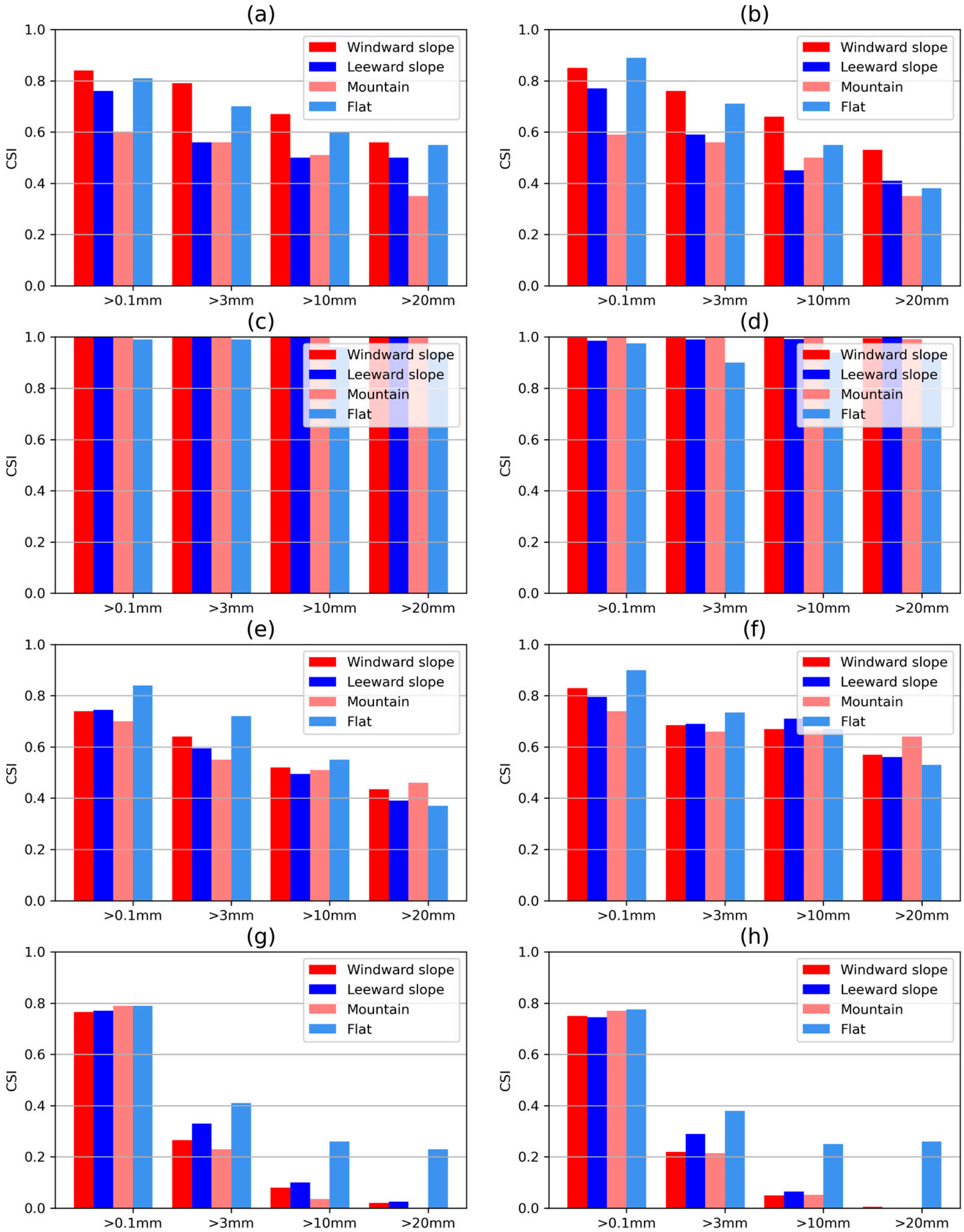

Figure 8. The critical success index (CSI) of the control experiments (**a**,**c**,**e**,**g**) and sensitivity experiments (**b**,**d**,**f**,**h**) based on the neighbourhood maximum (NM) method for three-hourly cumulative precipitation forecasts of light, moderate, heavy, and torrential rainfall during the test period. (**a**,**b**) HOTA; (**c**,**d**) LEKIMA; (**e**,**f**) HAGUPIT; (**g**,**h**) INFA.

4. Conclusions and Discussion

The GRIST model was used to carry out two types of simulation experiments for Typhoon HOTA, LEKIMA, HAGUPIT, and INFA, respectively. The difference between these two types of experiments lies in whether or not to reduce the degree of smoothness of the terrain so as to make it closer to the terrain's real-life state. For this paper, based on the precipitation distributions and typhoon centre locations of the four typhoon examples at each time period, the time periods with larger precipitation before and after the landfall of each typhoon were selected, and the area less than 400 km from the typhoon centre at each moment and with positive altitude was assessed. In addition, we divided the hills and flats with a threshold of 500 m. We used the topographic data to calculate the slope direction and divided the windward and leeward slopes by combining the wind field and the height of the terrain. The cumulative precipitation changes for different terrains at different precipitation thresholds were counted, and the level of model precipitation simulation was evaluated. The results of the present study indicate the following:

(1) Compared to the experiment before the improved topography, the model after the improved topography simulated more precipitation. The improved experiments consistently simulated the area of large-value cumulative precipitation during the study period and were more in line with the observations. The temporal trend of the three-hourly cumulative precipitation was more consistent with the observed precipitation. Typhoon HAGUPIT had the best modelled change in three-hourly cumulative precipitation among the four individual typhoon cases.
(2) The simulated precipitation deviation was smallest for Typhoon HAGUPIT and largest for Typhoon LEKIMA. Reducing the degree of terrain smoothing can mitigate the model's simulated precipitation bias for Typhoon LEKIMA, but it may inadvertently increase the model's precipitation bias for other typhoon individual typhoon cases. The influence of topographic factors is evident as simulated precipitation deviations are consistently larger in mountainous areas than in flat areas. However, the precipitation deviations on the windward and leeward slopes vary among different typhoon events.
(3) Improved terrain not only enhances the number of hits but also reduces the spatial bias in typhoon precipitation, thereby improving forecasts. The topographic differences between flat and mountainous terrain are much more pronounced than the effect of topographic differences between the windward and leeward slopes on model-simulated precipitation. There is a significant bias in the spatial distribution of precipitation over mountains, and the model provides better precipitation simulations for flat terrain. The impact of the windward and leeward slopes on precipitation simulation varies among different typhoon cases. Precipitation simulations for a wide range of terrains with large precipitation thresholds are slightly inadequate. However, for Typhoon HOTA, after improving the terrain to enhance its precipitation simulation, it has the capability to forecast heavy rainfall scenarios in mountainous areas.

It should be noted that this paper only analyses the precipitation simulation characteristics of the four typhoon cases in terms of two terrain factors, namely the windward/leeward slopes and mountainous/flat terrain. From the results of this study, it is easy to see that the effects of certain topographic factors on typhoon precipitation vary greatly from one typhoon to another, which may be due to the fact that factors such as typhoon intensity and structure synergistically influence typhoon precipitation with topographic factors, resulting in a huge difference in the effects of the windward/leeward slopes on typhoon precipitation. Therefore, the study sample can be increased to further investigate the commonality of effects for different topographic factors on typhoon precipitation in future. On the other hand, the physical mechanisms of typical typhoon cases affected by topographic factors need to be investigated further.

Author Contributions: Conceptualization, X.-Z.C. and Y.-L.M.; Methodology, X.-Z.C. and Y.-L.M.; Software, X.-Z.C. and C.-Q.L.; Validation, X.-Z.C.; Formal analysis, X.-Z.C., Y.-L.M., C.-Q.L. and L.-L.F.; Investigation, X.-Z.C. and Y.-L.M.; Resources, L.-L.F.; Data curation, X.-Z.C. and Y.-L.M.; Writing—original draft, X.-Z.C.; Writing—review and editing, X.-Z.C.; Visualization, X.-Z.C.; Supervision, Y.-L.M.; Project administration, Y.-L.M.; Funding acquisition, Y.-L.M. All authors have read and agreed to the published version of the manuscript.

Funding: This research was funded by National Key Research and Development Program of China, grant number No. 2021YFC3000804.

Institutional Review Board Statement: Not applicable.

Informed Consent Statement: Not applicable.

Data Availability Statement: Data used in this study can be downloaded from the websites below: Best Track Archive for Climate Stewardship (IBTrACS): https://www.ncei.noaa.gov/products/international-best-track-archive?name=ib-v4-access (accessed on 15 May 2023); GPM IMERG Final Precipitation data: https://disc.gsfc.nasa.gov/datasets/GPM_3IMERGHH_06/summary?keywords=%22IMERG%20final%22 (accessed on 21 May 2023); The topographic data: https://asterweb.jpl.nasa.gov/gdem.asp (accessed on 31 May 2022).

Conflicts of Interest: The authors declare no conflict of interest.

References

1. Lackmann, G.M. Hurricane Sandy before 1900 and after 2100. *Bull. Am. Meteorol. Soc.* **2015**, *96*, 547–560. [CrossRef]
2. Wang, D.; Wang, X.; Liu, L.; Wang, D.; Huang, H.; Pan, C. Evaluation of CMPA precipitation estimate in the evolution of typhoon-related storm rainfall in Guangdong, China. *J. Hydroinform.* **2016**, *18*, 1055–1068. [CrossRef]
3. Abancó, C.; Bennett, G.L.; Matthews, A.J.; Matera, M.A.M.; Tan, F.J. The role of geomorphology, rainfall and soil moisture in the occurrence of landslides triggered by 2018 Typhoon Mangkhut in the Philippines. *Nat. Hazards Earth Syst. Sci.* **2021**, *21*, 1531–1550. [CrossRef]
4. Gao, Y.; Zhang, Y.; Lei, L.; Tang, J. Multi-scale characteristics of an extreme rain event in Shandong Province, produced by Typhoon Lekima (2019). *Front. Earth Sci.* **2023**, *10*, 1093545. [CrossRef]
5. Wu, Y.-C.; Yang, M.-J.; Rogers, R.F. Examining Terrain Effects on the Evolution of Precipitation and Vorticity of Typhoon Fanapi (2010) after Departing the Central Mountain Range of Taiwan. *Mon. Weather Rev.* **2022**, *150*, 1517–1540. [CrossRef]
6. Fang, X.; Kuo, Y.-H.; Wang, A. The impacts of Taiwan topography on the predictability of Typhoon Morakot's record-breaking rainfall: A high-resolution ensemble simulation. *Weather Forecast.* **2011**, *26*, 613–633. [CrossRef]
7. Yang, M.J.; Zhang, D.L.; Tang, X.D.; Zhang, Y. A modeling study of Typhoon Nari (2001) at landfall: 2. Structural changes and terrain-induced asymmetries. *J. Geophys. Res. Atmos.* **2011**, *116*, D09112. [CrossRef]
8. Li, D.Y.; Huang, C.Y. The influences of orography and ocean on track of Typhoon Megi (2016) past Taiwan as identified by HWRF. *J. Geophys. Res. Atmos.* **2018**, *123*, 492–511, 517. [CrossRef]
9. Cho, W.; Park, J.; Moon, J.; Cha, D.-H.; Moon, Y.-m.; Kim, H.-S.; Noh, K.-j.; Park, S.-H. Effects of topography and sea surface temperature anomalies on heavy rainfall induced by Typhoon Chaba in 2016. *Geosci. Lett.* **2022**, *9*, 29. [CrossRef]
10. Liu, J.; Li, Z.; Xu, M. Analysis of terrain height effects on the asymmetric precipitation patterns during the landfall of typhoon Meranti (2010). *Atmos. Clim. Sci.* **2019**, *9*, 331. [CrossRef]
11. Yu, Z.-f.; Yu, H.; Gao, S.-t. Terrain impact on the precipitation of landfalling Typhoon Talim. *J. Trop. Meteorol.* **2010**, *16*, 115.
12. Ping, O.; Yong-Qing, W.; Xiu-Nian, Z.; Li, T. A Numerical Study of Mesoscale-Topography Influence on the Heavy Rainband of Typhoon Hato (2017). *J. Trop. Meteorol.* **2021**, *27*, 393–405. [CrossRef]
13. Jolliffe, I.T.; Stephenson, D.B. *Forecast Verification: A Practitioner's Guide in Atmospheric Science*; John Wiley & Sons: Hoboken, NJ, USA, 2012.
14. Brill, K.F.; Mesinger, F. Applying a general analytic method for assessing bias sensitivity to bias-adjusted threat and equitable threat scores. *Weather Forecast.* **2009**, *24*, 1748–1754. [CrossRef]
15. Schaefer, J.T. The critical success index as an indicator of warning skill. *Weather Forecast.* **1990**, *5*, 570–575. [CrossRef]
16. Yu, B.; Zhu, K.; Xue, M.; Zhou, B. Using new neighborhood-based intensity-scale verification metrics to evaluate WRF precipitation forecasts at 4 and 12 km grid spacings. *Atmos. Res.* **2020**, *246*, 105117. [CrossRef]
17. Mittermaier, M.; Roberts, N.; Thompson, S.A. A long-term assessment of precipitation forecast skill using the fractions skill score. *Meteorol. Appl.* **2013**, *20*, 176–186. [CrossRef]
18. Mittermaier, M.; Roberts, N. Intercomparison of spatial forecast verification methods: Identifying skillful spatial scales using the fractions skill score. *Weather Forecast.* **2010**, *25*, 343–354. [CrossRef]
19. Atger, F. Verification of intense precipitation forecasts from single models and ensemble prediction systems. *Nonlinear Process. Geophys.* **2001**, *8*, 401–417. [CrossRef]
20. Casati, B. New developments of the intensity-scale technique within the Spatial Verification Methods Intercomparison Project. *Weather Forecast.* **2010**, *25*, 113–143. [CrossRef]
21. Keil, C.; Craig, G.C. A displacement and amplitude score employing an optical flow technique. *Weather Forecast.* **2009**, *24*, 1297–1308. [CrossRef]
22. Venugopal, V.; Basu, S.; Foufoula-Georgiou, E. A new metric for comparing precipitation patterns with an application to ensemble forecasts. *J. Geophys. Res. Atmos.* **2005**, *110*, D08111. [CrossRef]
23. Gilleland, E.; Ahijevych, D.; Brown, B.G.; Casati, B.; Ebert, E.E. Intercomparison of spatial forecast verification methods. *Weather Forecast.* **2009**, *24*, 1416–1430. [CrossRef]
24. Ebert, E.E. Neighborhood verification: A strategy for rewarding close forecasts. *Weather Forecast.* **2009**, *24*, 1498–1510. [CrossRef]
25. Schwartz, C.S. A comparison of methods used to populate neighborhood-based contingency tables for high-resolution forecast verification. *Weather Forecast.* **2017**, *32*, 733–741. [CrossRef]

26. Stein, J.; Stoop, F. Neighborhood-based contingency tables including errors compensation. *Mon. Weather Rev.* **2019**, *147*, 329–344. [CrossRef]
27. Clark, A.J.; Gallus, W.A.; Weisman, M.L. Neighborhood-based verification of precipitation forecasts from convection-allowing NCAR WRF model simulations and the operational NAM. *Weather Forecast.* **2010**, *25*, 1495–1509. [CrossRef]
28. Shao, D.; Zhang, Y.; Xu, J.; Zhang, H.; Chen, S.; Tu, S. Comparison between Multi-Physics and Stochastic Approaches for the 20 July 2021 Henan Heavy Rainfall Case. *Atmosphere* **2022**, *13*, 1057. [CrossRef]
29. Wang, C.-C.; Paul, S.; Huang, S.-Y.; Wang, Y.-W.; Tsuboki, K.; Lee, D.-I.; Lee, J.-S. Typhoon quantitative precipitation forecasts by the 2.5 km CReSS model in Taiwan: Examples and role of topography. *Atmosphere* **2022**, *13*, 623. [CrossRef]
30. Li, Y.; Wang, Y.; Lin, Y.; Fei, R.; Gao, J. Effects of terrain and landmass near Fujian Province of China on the structure and propagation of a long-lived rainband in Typhoon Longwang (2005): A numerical study. *J. Geophys. Res. Atmos.* **2020**, *125*, e2020JD033393. [CrossRef]
31. Li, Y.; Huang, W.; Zhao, J. Roles of mesoscale terrain and latent heat release in typhoon precipitation: A numerical case study. *Adv. Atmos. Sci.* **2007**, *24*, 35–43. [CrossRef]
32. Kuang, L.; Tian, M.; Li, Q.; Pang, Y.; Liu, X.; Tao, X. Analysis of Temporal and Spatial Variation Characteristics of Short-term Heavy Precipitation in Chongqing Based on Different Landforms (in Chinese). *Water Resour. Power* **2023**, *41*, 1–4.
33. Wang, J.; Zhang, M.; Ren, S.; Wang, X.; Miao, C. Simulation study on the impact of Taihang Mountain slopes on downhill front cyclone rainstorm (in Chinese). *Adv. Earth Sci.* **2019**, *34*, 717–730.
34. Zhou, X.; Gao, W.; Wu, Y.; Qian, Z.; Qiu, S. Quantitative study on the influence of terrain aspect and gradient on the precipitation distribution in Ya'an (in Chinese). *J. Meteorol. Sci.* **2019**, *39*, 322–335.
35. Li, X.; Zhang, Y.; Peng, X.; Li, J. Using a single column model (SGRIST1.0) for connecting model physics and dynamics in the Global-to-Regional Integrated forecast SysTem (GRIST-A20.8). *Geosci. Model Dev. Discuss.* **2020**, 1–28. [CrossRef]
36. Duc, L.; Saito, K.; Seko, H. Spatial-temporal fractions verification for high-resolution ensemble forecasts. *Tellus A Dyn. Meteorol. Oceanogr.* **2013**, *65*, 18171. [CrossRef]
37. Roberts, N. Assessing the spatial and temporal variation in the skill of precipitation forecasts from an NWP model. *Meteorol. Appl. A J. Forecast. Pract. Appl. Train. Tech. Model.* **2008**, *15*, 163–169. [CrossRef]
38. Roberts, N.M.; Lean, H.W. Scale-selective verification of rainfall accumulations from high-resolution forecasts of convective events. *Mon. Weather Rev.* **2008**, *136*, 78–97. [CrossRef]
39. English, J.M.; Turner, D.D.; Alcott, T.I.; Moninger, W.R.; Bytheway, J.L.; Cifelli, R.; Marquis, M. Evaluating operational and experimental HRRR model forecasts of atmospheric river events in California. *Weather Forecast.* **2021**, *36*, 1925–1944. [CrossRef]